



SpatialThinker: Reinforcing 3D Reasoning in Multimodal LLMs via Spatial Rewards

Anonymous Author(s)

Affiliation

Address

email

Abstract

1 Multimodal large language models (MLLMs) have achieved remarkable progress
2 in vision–language tasks, but they continue to struggle with spatial understanding.
3 Existing spatial MLLMs often rely on explicit 3D inputs or architecture-specific
4 modifications, and remain constrained by large-scale datasets and sparse supervision.
5 To address these limitations, we introduce SPATIALTHINKER, a 3D-aware
6 MLLM trained with RL to integrate structured spatial grounding with multi-step
7 reasoning. The model simulates human-like spatial perception by constructing
8 a scene graph that captures task-relevant objects and spatial relations, and then
9 reasons via dense spatial reward supervision. SPATIALTHINKER builds on two key
10 innovations: (1) a data synthesis pipeline that generates STVQA-7K, a high-quality
11 spatial VQA dataset, and (2) online RL with a multi-objective dense spatial re-
12 ward enforcing spatial grounding. SPATIALTHINKER-7B outperforms supervised
13 fine-tuning and the sparse RL baseline across six spatial understanding bench-
14 marks, nearly doubling the base-model gain compared to sparse RL (+6.5% vs.
15 +3.6%), and matches or surpasses GPT-4o. These results showcase the effective-
16 ness of combining spatial supervision with reward-aligned reasoning in enabling
17 robust 3D spatial understanding with limited data and advancing MLLMs towards
18 human-level visual reasoning.

1 Introduction

20 Spatial reasoning is central to human intelligence, enabling us to perceive, localize, and manipulate
21 objects in complex environments. This ability is critical for embodied AI tasks such as robotic
22 manipulation [35, 23, 56], navigation [31], and augmented reality [38], where spatial awareness
23 underpins real-world decision-making [19, 66]. While multimodal large language models (MLLMs)
24 excel at general vision–language tasks [34, 45, 17, 5, 20, 47, 25], they continue to struggle with
25 3D spatial understanding [8, 68, 36, 80, 67, 51], which requires capturing geometry, structure, and
26 relations beyond 2D projections.

27 Existing approaches remain data-hungry or architecturally specialized. They rely on massive synthetic
28 datasets derived from 3D scene graphs (e.g., SpatialVLM was trained on 2B Spatial VQA samples,
29 SpatialRGPT on 700k) [8, 15, 13], architectural changes [30], explicit 3D inputs such as point clouds
30 [29, 13, 6], or reinforcement learning (RL) with sparse rewards [53, 70, 77, 78, 63, 88].

31 We present SPATIALTHINKER, a 3D-aware MLLM that integrates scene graph grounding with
32 multi-step reasoning through online policy RL. The model builds question-focused scene subgraphs
33 consisting of objects, their relations, and localized coordinates, and reasons over them under a
34 lexicographically-ordered multi-objective reward: format rewards enforce structured reasoning,
35 count penalties regulate regional focus, accuracy rewards prioritize correctness, and CIoU-based

36 spatial rewards encourage precise localization. This design promotes human-like reasoning: observe,
37 localize, think, answer.

38 Despite training on only 7K samples with our synthesized STVQA-7K dataset, SPATIALTHINKER-7B
39 outperforms supervised fine-tuning (+7.2%) and sparse RL baseline (+2.9%) across six benchmarks,
40 and matches or surpasses GPT-4o (+1.7%) [34], with a +12.1% gain on 3DSRBench [51]. While
41 sparse RL improves the base model by 3.6%, our dense spatial reward design yields 6.5%, nearly
42 doubling the benefit. These results show that models can learn effective spatial reasoning by focusing
43 on relevant regions, constructing internal scene representations, and accurately localizing objects
44 through dense, visually grounded rewards, without relying on large-scale data alone [8, 50].

45 Our contributions are:

- 46 • SPATIALTHINKER, a Spatial MLLM that integrates scene graph-based grounding with
47 online RL for spatial reasoning, achieving strong results with only 7K samples.
- 48 • STVQA-7K, a high-quality spatial VQA dataset grounded in scene graphs.
- 49 • A dense, lexicographically gated multi-objective reward that guides regionally focused
50 spatial reasoning, achieving superior generalization across six spatial benchmarks.

51 2 SpatialThinker: Spatially-Aware Reasoning MLLMs

52 2.1 Multi-Objective Reward Design

53 SPATIALTHINKER is trained with a fine-grained, multi-objective reward that guides visually grounded
54 reasoning. Unlike prior RLVR methods relying on sparse correctness signals [58, 88, 64], we combine
55 four complementary components, including: format, accuracy, count, and spatial rewards, which is
56 aligned with the reasoning stages: observe, localize, think, answer.

57 **Format Reward.** Responses must follow a structured template with $\langle \text{observe} \rangle$, $\langle \text{scene} \rangle$, $\langle \text{think} \rangle$,
58 and $\langle \text{answer} \rangle$ tags. The scene JSON must be parseable, with valid object fields (ID, bbox) and
59 triplet relations. The format reward $R_f \in \{0, 1\}$ (weight $w_{\text{format}} = 0.1$) enforces this structure.

60 **Accuracy Reward.** To prioritize task performance, we assign $R_a = 1$ if the predicted answer exactly
61 matches the ground truth, else 0. This component receives the highest weight ($w_{\text{accuracy}} = 0.5$) to
62 prioritize task performance while the other rewards guide how the model arrives at correct answers.

63 **Count Reward.** The count reward encourages the model to predict the appropriate number of
64 objects and relations relevant to the spatial query. It penalizes both under- and over-generation,
65 using a weighted error term based on the deviation between predicted and ground-truth counts:
66 $R_c = w_{\text{count}} \cdot (0.7 \cdot \text{obj-score} + 0.3 \cdot \text{rel-score})$, where $w_{\text{count}} = 0.2$. This guides the model to
67 stay focused on question-relevant regions. Without it, models tend to game the spatial reward by
68 generating excessive objects and relations to boost match likelihood.

69 **Spatial Reward.** To supervise object localization, we compute the spatial reward only when the final
70 answer is correct. Predicted and ground-truth objects are matched using the Hungarian algorithm
71 with a cost function that combines Complete IoU (CIoU) and semantic similarity: $C(o_i^{\text{pred}}, o_j^{\text{gt}}) =$
72 $\lambda_{\text{spatial}}(1 - \text{IoU}(b_i, b_j)) + \lambda_{\text{semantic}}(1 - \text{sim}(l_i, l_j))$, where b and l denote bounding boxes and labels,
73 respectively. The reward is then computed as the average CIoU across matched pairs: $R_{\text{spatial}} =$
74 $\frac{1}{|\mathcal{M}|} \sum_{(i,j) \in \mathcal{M}} \text{CIoU}(b_i^{\text{pred}}, b_j^{\text{gt}})$; $w_{\text{spatial}} = 0.2$. CIoU offers dense supervision over IoU, even for
75 non-overlapping boxes by incorporating distance and aspect ratio terms [86].

76 **Lexicographic Gating.** To avoid reward gaming across objectives, we apply lexicographic ordering
77 with conditional gating [65], prioritizing format $\succ \{\text{count}, \text{accuracy}\} \succ \text{spatial}$. The model must first
78 satisfy formatting, then jointly optimize count and accuracy, and receives spatial reward only when
79 the answer is correct. This ensures spatial grounding reinforces valid reasoning. Without accuracy
80 gating, we observe that models overfit to spatial localization while sacrificing task correctness. The
81 final reward is computed as the following with $\mathbb{I}[\cdot]$ as the indicator function:

$$R_{\text{total}} = \mathbb{I}[R_{\text{format}} > 0] \cdot (w_f R_f + w_c R_c + w_a R_a + \mathbb{I}[R_{\text{accuracy}} > 0] \cdot w_s R_s)$$

82 **2.2 Online RL Policy Optimization**

83 To train SPATIALTHINKER with dense, lexicographically gated rewards, we adopt Group-Relative
 84 Policy Optimization (GRPO) [16, 62], an online RL method that avoids critic networks by esti-
 85 mating advantages through intra-group comparisons. Given an input \mathbf{x} , we sample G trajectories
 86 $\{y^{(1)}, \dots, y^{(G)}\}$ from the current policy $\pi_{\theta_{\text{old}}}$. Each is scored via the reward function (Section 2.1),
 87 and advantages are computed using group-normalized scores: $A^{(i)} = \frac{r^{(i)} - \mu}{\sigma + \varepsilon}$, where μ and σ are the
 88 group mean and standard deviation, and $\varepsilon = 10^{-6}$. We then update the policy using a PPO-style
 89 clipped loss with KL regularization:

$$\mathcal{L}_{\text{RL}}(\theta) = -\frac{1}{G} \sum_{i=1}^G \frac{1}{|y^{(i)}|} \sum_{t=1}^{|y^{(i)}|} \left[\min \left(r^{i,t} A^{(i)}, \text{clip}(r^{i,t}, 1 - \epsilon_l, 1 + \epsilon_h) A^{(i)} \right) - \beta D_{\text{KL}}^{i,t} \right],$$

90 where $r^{i,t} = \frac{\pi_{\theta}(y_t^{(i)} | \mathbf{x}, y_{<t}^{(i)})}{\pi_{\theta_{\text{old}}}(y_t^{(i)} | \mathbf{x}, y_{<t}^{(i)})}$ is the importance ratio between new and old policies, and $D_{\text{KL}}^{i,t}$ is the
 91 token-level KL divergence against a reference model. We set $\epsilon_l = 0.2$, $\epsilon_h = 0.3$, and $\beta = 10^{-2}$.
 92 This loss encourages learning from dense supervision while controlling policy drift for stability and
 93 generalization.

94 **2.3 STVQA-7K: Dataset Construction**

95 To facilitate reward-aligned spatial reasoning, we construct STVQA-7K, a synthetic visual question
 96 answering (VQA) dataset built from human-annotated scene graphs in Visual Genome [39]. STVQA-
 97 7K comprises 7,587 spatially grounded multiple-choice VQA pairs spanning both 2D and 3D
 98 spatial understanding. We augment the original VG150 predicate set with 34 additional spatial
 99 relations—covering distance (e.g., near, far), size (e.g., bigger, taller), orientation (e.g., facing away),
 100 and containment (e.g., inside, beneath)—to enrich the relational vocabulary beyond the standard 50
 101 predicates. Each QA pair is generated from a scene graph using Claude Sonnet 4 [4], then verified
 102 for semantic correctness using GPT-4o [34] through a consistency-based filtering pipeline. From an
 103 initial pool of 56,224 questions, we retain the top 7.5K high-quality samples after automated rating,
 104 difficulty estimation, and validation. Finally, we align each question with a subgraph of relevant
 105 objects and relations, enabling localized scene graph supervision during training. This results in
 106 a richly annotated, task-aligned dataset for developing and evaluating grounded spatial reasoning
 107 models. Complete data construction details are provided in Appendix C.

108 **3 Experiments**

109 **Implementation Details.** We build SPATIALTHINKER upon two strong open-source multimodal
 110 base models: Qwen2.5-VL-3B and Qwen2.5-VL-7B [5]. No supervised fine-tuning is performed
 111 prior to RL training on our STVQA-7K dataset (Section C). We employ GRPO [62] as the advantage
 112 estimator as described in Section 2.2, using a rollout size of 8 samples per query and a sampling
 113 temperature of 1.0. The models are trained with a maximum context length of 16,384 tokens. The
 114 rollout batch size is set to 512, and the global batch size is 128. We train for 75 training steps i.e., 5
 115 training episodes) on $4 \times$ NVIDIA H100 80GB GPUs. Training time totals around 13 hours for the
 116 3B model and 15 hours for the 7B model. The models are trained on high-resolution image inputs
 117 ranging from 512×512 to 2048×2048 pixels, to preserve fine-grained spatial information. All
 118 model parameters, including the vision encoder, are updated during training. We use the AdamW
 119 optimizer with bf16 precision, a learning rate of 1×10^{-6} , and a weight decay of 1×10^{-2} . The KL
 120 penalty coefficient is set to 10^{-2} . STVQA-7K is partitioned with a 90/10 train-validation split.

121 **Experimental Setup.** We evaluate SPATIALTHINKER on six spatial reasoning benchmarks span-
 122 ning 2D and 3D understanding: CV-Bench [67], BLINK [21], 3DSRBench [51], MMVP [68],
 123 SpatialBench [6], and RealWorldQA [76]. Comparisons include both proprietary (GPT-4o [34])
 124 and open-source models—Qwen2.5-VL [5], Cambrian-1 [67], LLaVA-Next [41], VLAA-Thinker
 125 [10]—as well as spatially-specialized models such as SpatialRGPT [13], SpatialBot [6], SpaceLLaVA
 126 [8], SpaceThinker [1], and RoboPoint [83]. We also evaluate training variants including supervised
 127 fine-tuning (SFT) and vanilla GRPO (using only format and accuracy rewards) to isolate the contri-
 128 bution of dense spatial rewards. Detailed experimental setup, evaluation settings, and prompts are
 129 shared in Appendix D

Model	3DSRBench [51]	CV-Bench [67]		Avg.	BLINK [21]		Avg.
		2D	3D		Spatial Relation	Relative Depth	
<i>Proprietary Models</i>							
GPT-4o [34]	44.3	75.8	83.0	79.4	82.5	78.2	80.4
<i>Open-Source General MLLMs</i>							
Qwen2.5-VL-3B [5]	44.0	59.9	60.2	60.1	66.4	54.0	60.2
Qwen2.5-VL-7B [5]	48.4	69.1	68.0	68.6	84.0	52.4	68.2
VLAA-Thinker-7B [10]	52.2	60.8	60.3	60.6	81.2	71.0	76.1
LLaVA-NeXT-3B [41]	48.4	62.2	65.3	63.8	-	-	-
Cambrian-1-8B [67]	42.2	72.3	72	72.2	-	-	-
<i>Open-Source Spatial MLLMs</i>							
RoboPoint-13B [83]	-	-	61.2	-	60.8	61.3	61.1
SpaceThinker-Qwen2.5-VL-3B [1]	51.1	65.1	65.9	65.5	73.4	59.9	66.7
SpaceLlaVA-13B [8]	42.0	-	68.5	-	72.7	62.9	67.8
SpatialBot-3B [6]	41.1	-	69.1	-	67.8	67.7	67.8
Spatial-RGPT-7B w/ depth [13]	48.4	-	60.7	-	65.7	82.3	74.0
<i>Method Comparison (Trained on STVQA-7K)</i>							
Qwen2.5-VL-3B + SFT	50.8	53.9	68.4	61.2	65.0	66.9	66.0
Qwen2.5-VL-3B + Vanilla GRPO	50.1	70.6	66.6	68.6	73.4	55.6	64.5
SpatialThinker-3B (Ours)	52.9	71.0	76.3	73.7	81.8	66.9	74.4
Qwen2.5-VL-7B + SFT	53.6	56.1	71.3	63.7	75.5	64.5	70.0
Qwen2.5-VL-7B + Vanilla GRPO	54.7	68.9	76.5	72.7	80.4	75.0	77.7
SpatialThinker-7B (Ours)	56.4	77.7	78.7	78.2	86.0	72.6	79.3

Table 1: Performance over 2D & 3D Spatial Understanding Benchmarks across different model types.

3.1 Results

Performance across spatial benchmarks. As shown in Tables 1, 2, SPATIALTHINKER-7B achieves strong performance across all benchmarks: 78.2% on CV-Bench (vs. GPT-4o’s 79.4%), 79.3% on BLINK tasks (vs. GPT-4o’s 80.4%), and 78.0% on MMVP (vs. GPT-4o’s 70.7%). On 3DSRBench, it scores 56.4%, outperforming GPT-4o by 12.1%, and achieves 66.4% on SpatialBench (vs. GPT-4o’s 67.0%). On RealWorldQA, it reaches 69.2%, demonstrating strong transfer to real-world spatial reasoning. Despite using only RGB inputs and 7K training samples, SPATIALTHINKER-7B matches or surpasses larger proprietary and spatially-specialized open-source models.

Comparison with training baselines. Compared to SFT and vanilla GRPO, SPATIALTHINKER-7B achieves +7.2% and +2.9% higher average accuracy, respectively. Similarly, the 3B variant shows +6.0% and +4.2% average gains over its SFT and GRPO baselines. Notably, vanilla GRPO improves +3.6% over the base model, while SPATIALTHINKER-7B trained with spatial rewards achieves +6.5%, nearly doubling the benefit. For the 3B model, vanilla GRPO yields a +5.6% average gain over the base, whereas SPATIALTHINKER-3B achieves +9.7%. This multiplicative effect with $\times 2$ improvement over the sparse RL baseline affirms that dense spatial rewards offer complementary learning signals that amplify reinforcement learning efficacy.

4 Conclusion

We introduced SPATIALTHINKER, a 3D-aware MLLM that achieves strong spatial reasoning by combining scene graph grounding with dense spatial rewards. Trained on just 7K samples, it matches or surpasses GPT-4o on spatial benchmarks while outperforming models trained on larger datasets and specialised spatial MLLMs. Dense spatial rewards nearly double the gains of standard RL, underscoring the value of rich supervision signals. While our approach relies on explicit scene graphs, future work could explore implicit spatial reasoning with latent tokens, and design unified multi-objective policies covering diverse visual tasks.

Model	MMVP [68]	SpatialBench [6]	RealWorldQA [76]	Proprietary and Open-Source MLLMs	
				Spatial Relation	Relative Depth
<i>Proprietary and Open-Source MLLMs</i>					
GPT-4o [34]	70.7	67.0	75.4		
Claude 3.5 Sonnet [3]	71.3	-	60.1		
Qwen2.5-VL-3B [5]	67.0	49.9	58.2		
Qwen2.5-VL-7B [5]	72.3	62.5	68.4		
SpaceThinker-Qwen2.5-VL-3B [1]	63.0	57.9	61.6		
VLAA-Thinker-7B [10]	75.3	66.2	66.4		
<i>Method Comparison (Trained on STVQA-7K)</i>					
Qwen2.5-VL-3B + SFT	62.7	56.3	64.8		
Qwen2.5-VL-3B + Vanilla GRPO	68.3	56.9	64.4		
SpatialThinker-3B (Ours)	69.0	61.5	66.3		
Qwen2.5-VL-7B + SFT	68.3	63.5	65.4		
Qwen2.5-VL-7B + Vanilla GRPO	74.3	64.2	66.6		
SpatialThinker-7B (Ours)	78.0	66.4	69.2		

Table 2: Results on additional spatial understanding & real-world tasks.

164 **References**

- 165 [1] Remyx AI and Salma Mayorquin. “SpaceThinker Models”. In: *Hugging Face* (Apr. 2025).
166 URL: <https://huggingface.co/remyxai/SpaceThinker-Qwen2.5VL-3B>.
- 167 [2] Anthropic. “Claude 3.7 Sonnet System Card”. In: *Anthropic* (Feb. 2025).
- 168 [3] Anthropic. “Model Card Addendum: Claude 3.5 Haiku and Upgraded Claude 3.5 Sonnet”. In:
169 *Anthropic* (Oct. 2024).
- 170 [4] Anthropic. “System Card: Claude Opus 4 & Claude Sonnet 4”. In: *Anthropic System Cards*
171 (May 2025).
- 172 [5] Shuai Bai et al. “Qwen2.5-VL Technical Report”. In: *ArXiv* abs/2502.13923 (2025).
- 173 [6] Wenxiao Cai et al. “Spatialbot: Precise spatial understanding with vision language models”.
174 In: *arXiv preprint arXiv:2406.13642* (2024).
- 175 [7] Nicolas Carion et al. “End-to-end object detection with transformers”. In: *European conference
on computer vision*. Springer. 2020, pp. 213–229.
- 177 [8] Boyuan Chen et al. “Spatialvlm: Endowing vision-language models with spatial reasoning
178 capabilities”. In: *Proceedings of the IEEE/CVF Conference on Computer Vision and Pattern
179 Recognition*. 2024, pp. 14455–14465.
- 180 [9] Guikun Chen, Jin Li, and Wenguan Wang. “Scene Graph Generation with Role-Playing Large
181 Language Models”. In: *ArXiv* abs/2410.15364 (2024).
- 182 [10] Hardy Chen et al. “SFT or RL? An Early Investigation into Training R1-Like Reasoning Large
183 Vision-Language Models”. In: *ArXiv* abs/2504.11468 (2025).
- 184 [11] Zuyao Chen et al. “Compile scene graphs with reinforcement learning”. In: *arXiv preprint
185 arXiv:2504.13617* (2025).
- 186 [12] Zuyao Chen et al. “Gpt4sgg: Synthesizing scene graphs from holistic and region-specific
187 narratives”. In: *arXiv preprint arXiv:2312.04314* (2023).
- 188 [13] An-Chieh Cheng et al. “Spatialrgpt: Grounded spatial reasoning in vision-language models”.
189 In: *Advances in Neural Information Processing Systems* 37 (2024), pp. 135062–135093.
- 190 [14] Yuren Cong, Michael Ying Yang, and Bodo Rosenhahn. “Reltr: Relation transformer for scene
191 graph generation”. In: *IEEE Transactions on Pattern Analysis and Machine Intelligence* 45.9
192 (2023), pp. 11169–11183.
- 193 [15] Erik Daxberger et al. “Mm-spatial: Exploring 3d spatial understanding in multimodal llms”.
194 In: *arXiv preprint arXiv:2503.13111* (2025).
- 195 [16] DeepSeek-AI et al. “DeepSeek-R1: Incentivizing Reasoning Capability in LLMs via Rein-
196forcement Learning”. In: *ArXiv* abs/2501.12948 (2025).
- 197 [17] Matt Deitke et al. “Molmo and pixmo: Open weights and open data for state-of-the-art vision-
198 language models”. In: *Proceedings of the Computer Vision and Pattern Recognition Conference*.
199 2025, pp. 91–104.
- 200 [18] Yihe Deng et al. “OpenVLthinker: Complex Vision-Language Reasoning via Iterative SFT-RL
201 Cycles”. In: 2025.
- 202 [19] Danny Driess et al. “PaLM-E: An Embodied Multimodal Language Model”. In: *International
203 Conference on Machine Learning*. 2023.
- 204 [20] Kimi Team Angang Du et al. “Kimi-VL Technical Report”. In: *ArXiv* abs/2504.07491 (2025).
- 205 [21] Xingyu Fu et al. “BLINK: Multimodal Large Language Models Can See but Not Perceive”. In:
206 *ArXiv* abs/2404.12390 (2024).
- 207 [22] Kanishk Gandhi et al. “Cognitive Behaviors that Enable Self-Improving Reasoners, or, Four
208 Habits of Highly Effective STaRs”. In: *ArXiv* abs/2503.01307 (2025).
- 209 [23] Jensen Gao et al. “Physically Grounded Vision-Language Models for Robotic Manipula-
210 tion”. In: *2024 IEEE International Conference on Robotics and Automation (ICRA)* (2023),
211 pp. 12462–12469.
- 212 [24] Gemini Team and Google. “Gemini 1.5: Unlocking Multimodal Understanding across Millions
213 of Tokens of Context”. In: *Google DeepMind* (2024).
- 214 [25] Google. “Gemini 2.0 Flash: Model Card”. In: *Technical Report* (Apr. 2025). Published April
215 15, 2025.
- 216 [26] Qiao Gu et al. “ConceptGraphs: Open-Vocabulary 3D Scene Graphs for Perception and
217 Planning”. In: *2024 IEEE International Conference on Robotics and Automation (ICRA)*
218 (2023), pp. 5021–5028.

- 219 [27] Marcel Hildebrandt et al. “Scene Graph Reasoning for Visual Question Answering”. In: *ArXiv*
 220 abs/2007.01072 (2020).
- 221 [28] Yining Hong et al. “3D concept learning and reasoning from multi-view images”. In: *Proceedings of the IEEE/CVF Conference on Computer Vision and Pattern Recognition*. 2023,
 222 pp. 9202–9212.
- 224 [29] Yining Hong et al. “3D-LLM: Injecting the 3D world into large language models”. In: *Advances
 225 in Neural Information Processing Systems* 36 (2023), pp. 20482–20494.
- 226 [30] Yining Hong et al. “3d-llm: Injecting the 3d world into large language models”. In: *Advances
 227 in Neural Information Processing Systems* 36 (2023), pp. 20482–20494.
- 228 [31] Chen Huang et al. “Visual Language Maps for Robot Navigation”. In: *2023 IEEE International
 229 Conference on Robotics and Automation (ICRA)* (2022), pp. 10608–10615.
- 230 [32] Wenzuan Huang et al. “Vision-R1: Incentivizing Reasoning Capability in Multimodal Large
 231 Language Models”. In: *ArXiv* abs/2503.06749 (2025).
- 232 [33] Drew A Hudson and Christopher D Manning. “Gqa: A new dataset for real-world visual rea-
 233 soning and compositional question answering”. In: *Proceedings of the IEEE/CVF conference
 234 on computer vision and pattern recognition*. 2019, pp. 6700–6709.
- 235 [34] Aaron Hurst et al. “Gpt-4o system card”. In: *arXiv preprint arXiv:2410.21276* (2024).
- 236 [35] Physical Intelligence et al. “π0.5: a Vision-Language-Action Model with Open-World Gener-
 237 alization”. In: *ArXiv* abs/2504.16054 (2025).
- 238 [36] Amita Kamath, Jack Hessel, and Kai-Wei Chang. “What’s” up” with vision-language models?
 239 investigating their struggle with spatial reasoning”. In: *arXiv preprint arXiv:2310.19785*
 240 (2023).
- 241 [37] Kibum Kim et al. “Llm4sgg: Large language models for weakly supervised scene graph
 242 generation”. In: *Proceedings of the IEEE/CVF Conference on Computer Vision and Pattern
 243 Recognition*. 2024, pp. 28306–28316.
- 244 [38] Mikhail Konenkov et al. “VR-GPT: Visual Language Model for Intelligent Virtual Reality
 245 Applications”. In: *ArXiv* abs/2405.11537 (2024).
- 246 [39] Ranjay Krishna et al. “Visual genome: Connecting language and vision using crowdsourced
 247 dense image annotations”. In: *International journal of computer vision* 123.1 (2017), pp. 32–
 248 73.
- 249 [40] Chengzu Li et al. “Topviewrs: Vision-language models as top-view spatial reasoners”. In:
 250 *arXiv preprint arXiv:2406.02537* (2024).
- 251 [41] Feng Li et al. “LLaVA-NeXT-Interleave: Tackling Multi-image, Video, and 3D in Large
 252 Multimodal Models”. In: *ArXiv* abs/2407.07895 (2024).
- 253 [42] Lin Li et al. “Relation-R1: Progressively Cognitive Chain-of-Thought Guided Reinforcement
 254 Learning for Unified Relation Comprehension”. In: *arXiv preprint arXiv:2504.14642* (2025).
- 255 [43] Lin Li et al. “Zero-shot Visual Relation Detection via Composite Visual Cues from Large
 256 Language Models”. In: *ArXiv* abs/2305.12476 (2023).
- 257 [44] Yanwei Li et al. “Mini-Gemini: Mining the Potential of Multi-modality Vision Language
 258 Models”. In: *ArXiv* abs/2403.18814 (2024).
- 259 [45] Ji Lin et al. “Vila: On pre-training for visual language models”. In: *Proceedings of the
 260 IEEE/CVF conference on computer vision and pattern recognition*. 2024, pp. 26689–26699.
- 261 [46] Haotian Liu et al. “Improved baselines with visual instruction tuning”. In: *Proceedings of the
 262 IEEE/CVF conference on computer vision and pattern recognition*. 2024, pp. 26296–26306.
- 263 [47] Haotian Liu et al. “Visual Instruction Tuning”. In: *ArXiv* abs/2304.08485 (2023).
- 264 [48] Yuqi Liu et al. “Seg-Zero: Reasoning-Chain Guided Segmentation via Cognitive Reinforce-
 265 ment”. In: *ArXiv* abs/2503.06520 (2025).
- 266 [49] Ziyu Liu et al. “Visual-RFT: Visual Reinforcement Fine-Tuning”. In: *ArXiv* abs/2503.01785
 267 (2025).
- 268 [50] Chenyang Ma et al. “Spatialpin: Enhancing spatial reasoning capabilities of vision-language
 269 models through prompting and interacting 3d priors”. In: *Advances in neural information
 270 processing systems* 37 (2024), pp. 68803–68832.
- 271 [51] Wufei Ma et al. “3DSRBench: A Comprehensive 3D Spatial Reasoning Benchmark”. In: *ArXiv*
 272 abs/2412.07825 (2024).

- 273 [52] Wufei Ma et al. “Spatialllm: A compound 3d-informed design towards spatially-intelligent
 274 large multimodal models”. In: *Proceedings of the Computer Vision and Pattern Recognition*
 275 Conference. 2025, pp. 17249–17260.
- 276 [53] Wufei Ma et al. “SpatialReasoner: Towards Explicit and Generalizable 3D Spatial Reasoning”.
 277 In: *ArXiv* abs/2504.20024 (2025).
- 278 [54] Fanqing Meng et al. “MM-Eureka: Exploring the Frontiers of Multimodal Reasoning with
 279 Rule-based Reinforcement Learning”. In: 2025.
- 280 [55] Roshanak Mirzaee et al. “Spartqa:: A textual question answering benchmark for spatial
 281 reasoning”. In: *arXiv preprint arXiv:2104.05832* (2021).
- 282 [56] Soroush Nasiriany et al. “PIVOT: Iterative Visual Prompting Elicits Actionable Knowledge for
 283 VLMs”. In: *ArXiv* abs/2402.07872 (2024).
- 284 [57] Michael Ogezi and Freda Shi. “SpaRE: Enhancing Spatial Reasoning in Vision-Language
 285 Models with Synthetic Data”. In: *arXiv preprint arXiv:2504.20648* (2025).
- 286 [58] Yi Peng et al. “LMM-R1: Empowering 3B LMMs with Strong Reasoning Abilities Through
 287 Two-Stage Rule-Based RL”. In: *ArXiv* abs/2503.07536 (2025).
- 288 [59] Zhiliang Peng et al. “Kosmos-2: Grounding multimodal large language models to the world”.
 289 In: *arXiv preprint arXiv:2306.14824* (2023).
- 290 [60] André Susano Pinto et al. “Tuning computer vision models with task rewards”. In: *ArXiv*
 291 abs/2302.08242 (2023).
- 292 [61] Hanoona Rasheed et al. “Glamm: Pixel grounding large multimodal model”. In: *Proceedings*
 293 of the IEEE/CVF Conference on Computer Vision and Pattern Recognition. 2024, pp. 13009–
 294 13018.
- 295 [62] Zhihong Shao et al. “DeepSeekMath: Pushing the Limits of Mathematical Reasoning in Open
 296 Language Models”. In: *ArXiv* abs/2402.03300 (2024).
- 297 [63] Chuming Shen et al. “SATORI-R1: Incentivizing Multimodal Reasoning with Spatial Ground-
 298 ing and Verifiable Rewards”. In: *ArXiv* abs/2505.19094 (2025).
- 299 [64] Haozhan Shen et al. “VLM-R1: A Stable and Generalizable R1-style Large Vision-Language
 300 Model”. In: *ArXiv* abs/2504.07615 (2025).
- 301 [65] Joar Skalse et al. “Lexicographic Multi-Objective Reinforcement Learning”. In: *ArXiv*
 302 abs/2212.13769 (2022).
- 303 [66] Gemini Robotics Team et al. “Gemini Robotics: Bringing AI into the Physical World”. In:
 304 *ArXiv* abs/2503.20020 (2025).
- 305 [67] Shengbang Tong et al. “Cambrian-1: A Fully Open, Vision-Centric Exploration of Multimodal
 306 LLMs”. In: *ArXiv* abs/2406.16860 (2024).
- 307 [68] Shengbang Tong et al. “Eyes wide shut? exploring the visual shortcomings of multimodal llms”.
 308 In: *Proceedings of the IEEE/CVF Conference on Computer Vision and Pattern Recognition*.
 309 2024, pp. 9568–9578.
- 310 [69] Johanna Wald et al. “Learning 3D Semantic Scene Graphs From 3D Indoor Reconstructions”.
 311 In: 2020 IEEE/CVF Conference on Computer Vision and Pattern Recognition (CVPR) (2020),
 312 pp. 3960–3969.
- 313 [70] Peiyao Wang and Haibin Ling. “SVQA-R1: Reinforcing Spatial Reasoning in MLLMs via
 314 View-Consistent Reward Optimization”. In: *ArXiv* abs/2506.01371 (2025).
- 315 [71] Peng Wang et al. “Qwen2-VL: Enhancing Vision-Language Model’s Perception of the World
 316 at Any Resolution”. In: *ArXiv* abs/2409.12191 (2024).
- 317 [72] Xingrui Wang et al. “3d-aware visual question answering about parts, poses and occlusions”.
 318 In: *Advances in Neural Information Processing Systems* 36 (2023), pp. 58717–58735.
- 319 [73] Xingrui Wang et al. “Compositional 4d dynamic scenes understanding with physics priors for
 320 video question answering”. In: *arXiv preprint arXiv:2406.00622* (2024).
- 321 [74] Zehan Wang et al. “SpatialCLIP: Learning 3D-aware Image Representations from Spatially
 322 Discriminative Language”. In: *Proceedings of the IEEE/CVF Conference on Computer Vision*
 323 and Pattern Recognition (CVPR) (2025), pp. 29656–29666. DOI: 10.1109/CVPR52734.2025.
 324 02761.
- 325 [75] Jason Wei et al. “Chain of Thought Prompting Elicits Reasoning in Large Language Models”.
 326 In: *ArXiv* abs/2201.11903 (2022).
- 327 [76] xAI. “Grok-1.5 Vision Preview”. In: *xAI Blog* (Apr. 2024).

- 328 [77] Jiaer Xia et al. "Visionary-R1: Mitigating Shortcuts in Visual Reasoning with Reinforcement
329 Learning". In: *ArXiv* abs/2505.14677 (2025).
- 330 [78] Tong Xiao et al. "Advancing Multimodal Reasoning Capabilities of Multimodal Large Lan-
331 guage Models via Visual Perception Reward". In: *ArXiv* abs/2506.07218 (2025).
- 332 [79] Yutaro Yamada et al. "Evaluating spatial understanding of large language models". In: *arXiv*
333 preprint arXiv:2310.14540 (2023).
- 334 [80] Jihan Yang et al. "Thinking in space: How multimodal large language models see, remember,
335 and recall spaces". In: *Proceedings of the Computer Vision and Pattern Recognition Conference*.
336 2025, pp. 10632–10643.
- 337 [81] Yi Yang et al. "R1-Onevision: Advancing Generalized Multimodal Reasoning through Cross-
338 Modal Formalization". In: *ArXiv* abs/2503.10615 (2025).
- 339 [82] Haoxuan You et al. "Ferret: Refer and ground anything anywhere at any granularity". In: *arXiv*
340 preprint arXiv:2310.07704 (2023).
- 341 [83] Wentao Yuan et al. "RoboPoint: A Vision-Language Model for Spatial Affordance Prediction
342 for Robotics". In: *ArXiv* abs/2406.10721 (2024).
- 343 [84] Yaowei Zheng et al. "EasyR1: An Efficient, Scalable, Multi-Modality RL Training Framework".
344 In: *arXiv* preprint arXiv:2501.12345 (2025).
- 345 [85] Yaowei Zheng et al. "LlamaFactory: Unified Efficient Fine-Tuning of 100+ Language Models".
346 In: *ArXiv* abs/2403.13372 (2024).
- 347 [86] Zhaohui Zheng et al. "Enhancing Geometric Factors in Model Learning and Inference for
348 Object Detection and Instance Segmentation". In: *IEEE Transactions on Cybernetics* 52 (2020),
349 pp. 8574–8586.
- 350 [87] Hengguang Zhou et al. "R1-Zero's "Aha Moment" in Visual Reasoning on a 2B Non-SFT
351 Model". In: *ArXiv* abs/2503.05132 (2025).
- 352 [88] Fangrui Zhu et al. "Struct2D: A Perception-Guided Framework for Spatial Reasoning in Large
353 Multimodal Models". In: *ArXiv* abs/2506.04220 (2025).

354 **Appendix**

355 **A Related Work**

356 **3D Spatial Reasoning in Multimodal Language Models.** While multimodal large language mod-
357 els have achieved notable success in fundamental visual tasks [34, 45, 17, 46], their ability to perform
358 complex spatial reasoning remains limited. Multiple evaluations have highlighted persistent shortcom-
359 ings in this domain [55, 68, 36, 79, 40, 80, 51], which can be partially attributed to the predominance
360 of datasets centered around visual perception rather than explicit spatial or relational grounding [33].
361 In response, considerable research has focused on incorporating 3D spatial information into MLLMs.
362 Early approaches embed explicit representations such as point clouds or multi-view reconstructions
363 [29, 28], while others generate structured spatial states or world models guided by physical priors [72,
364 73]. More recent systems have trained large-scale models with 3D-enhanced VQA datasets, such as
365 SpatialVLM with 2B samples [8], and extensions like SpatialPIN [50] or SpatialBot [6], which inject
366 3D priors or auxiliary depth signals. SpatialRGPT [13] builds 3D scene graphs from RGB-depth data
367 to produce a large 700k-sample spatial QA dataset for training, improving performance but requiring
368 extensive pre-processing and data. Similarly, MM-Spatial [15], SpatialLLM [52], and SpaRE [57]
369 address spatial reasoning with hundreds of thousands to millions of synthetic or reconstructed samples.
370 Despite this progress, existing methods are either data-heavy, reliant on specialized 3D inputs, or
371 restricted in modeling structured relational understanding. In contrast, SPATIALTHINKER achieves
372 robust 3D spatial reasoning including object localization, and relational and regional understanding,
373 using only 7K high-quality structured QA samples combined with reinforcement learning over dense
374 spatial rewards.

375 **Structured Visual Grounding in MLLMs.** Scene graphs provide a structured representation of
376 objects and their relations and have been widely explored for visual reasoning [27, 69, 26]. Classical
377 scene graph generation builds on detection-relation pipelines [7, 14], but often struggles with multi-
378 role or open-vocabulary reasoning. With the advent of LLMs, text-augmented approaches such as
379 LLM4SGG and GPT4SGG convert captions into structured graphs [37, 12], while more advanced
380 open-vocabulary SGG methods leverage VLMs or MLLMs to generalize beyond fixed ontologies
381 [9, 43]. Recent RL-driven frameworks, such as R1-SGG and Relation-R1, train models to construct
382 scene graphs directly with dense structural or cognitive rewards [11, 42], highlighting the utility of
383 structured supervision. In parallel, region-aware MLLMs like KOSMOS-2 [59], Ferret [82], and
384 GLaMM [61] improve spatial grounding by integrating region information through bounding boxes
385 and textual region descriptions, enabling more precise localization within images. SPATIALTHINKER
386 builds on these advances by explicitly grounding reasoning on scene subgraphs focused on the
387 question-specific region of interest, combining structured scene understanding with interpretable,
388 reward-guided spatial reasoning.

389 **Multimodal Reinforcement Learning.** Reinforcement learning (RL) has been widely adopted to
390 enhance reasoning in MLLMs, extending chain-of-thought prompting [75] and fine-grained verifiable
391 rewards to multimodal reasoning tasks. Recent works have applied RL for math reasoning [81,
392 54], classification and grounding [49], semantic segmentation [48], structured reasoning pipelines
393 [63] or referring expressions comprehension and open vocabulary detection [64, 60, 49]. Spatial
394 RL strategies have emerged as well: SVQA-R1 incorporates view-consistency rewards [70], while
395 SpatialReasoner adds coordinate-aware supervision in reasoning [64, 53]. Despite these efforts, most
396 existing methods rely on relatively simple or sparse reward signals, such as final answer accuracy
397 or coarse coordinate supervision, which provide limited guidance for detailed spatial relational
398 reasoning. SPATIALTHINKER advances this space with a fine-grained multi-objective reward design
399 covering regional subgraph construction, comprising object localisation and relational grounding,
400 and final correctness. The model predicts these structured representations first, then reasons over
401 them for detailed and interpretable spatial inference.

402 **B Preliminaries**

403 **Scene Graph Generation.** A scene graph provides a structured representation of an image I as a
404 directed graph $G = (V, E)$. Each node $v_i \in V$ denotes an object with a category label c_i and a 2D
405 bounding box $b_i = (x_i, y_i, w_i, h_i)$; each edge $e_{ij} \in E$ is a relationship triplet $\langle v_i, r_{ij}, v_j \rangle$ capturing

406 spatial or interactive relations (e.g., *left of*, *on*, *under*) [27, 69]. Classical SGG decomposes prediction
 407 into object detection and relation recognition [7, 14], while open-vocabulary methods leverage
 408 language/vision priors to generalize beyond fixed ontologies [9, 43]. We refer to *question-focused*
 409 *scene subgraphs* as $G_q = (V_q, E_q) \subseteq G$ that retain only objects and relations relevant to a given
 410 query q .

411 **Reasoning in Multimodal Large Language Models.** Multimodal large language models (MLLMs)
 412 define autoregressive policies π_θ over sequences of interleaved visual and textual tokens. Given an
 413 image \mathbf{x}_{img} and a spatial question \mathbf{x}_{text} , the model generates a reasoning trace $\mathbf{y} = (a_1, \dots, a_T)$,
 414 where each a_t represents a token from intermediate reasoning steps or the final answer. This policy is
 415 factorized as:

$$\pi_\theta(\mathbf{y} \mid \mathbf{x}_{\text{img}}, \mathbf{x}_{\text{text}}) = \prod_{t=1}^T \pi_\theta(a_t \mid \mathbf{x}_{\text{img}}, \mathbf{x}_{\text{text}}, a_{<t}) \quad (1)$$

416 While supervised fine-tuning enables models to imitate reasoning traces observed during training,
 417 reinforcement learning offers a principled way to optimize generation using explicit reward signals,
 418 often resulting in better generalization to out-of-distribution inputs and improved adherence to task-
 419 specific structure [22, 16, 32]. The reinforcement learning objective seeks to maximize expected
 420 reward over trajectories:

$$\max_{\theta} \mathbb{E}_{Q \sim \mathcal{D}, \mathbf{y} \sim \pi_\theta(\cdot \mid Q)} [R(Q, \mathbf{y})] \quad (2)$$

421 where $Q = \{\mathbf{x}_{\text{img}}, \mathbf{x}_{\text{text}}\}$ is the input query, \mathcal{D} is the dataset distribution, and R is a verifiable reward
 422 function evaluating task correctness, formatting, and spatial grounding.

423 **Task Formulation** We cast spatial reasoning in MLLMs as the task of producing a visually
 424 grounded response \mathbf{y} to a query $Q = \mathbf{x}_{\text{img}}, \mathbf{x}_{\text{text}}$. Unlike generic reasoning, our formulation explicitly
 425 requires constructing question-focused scene subgraphs G_q and reasoning over objects, bounding
 426 boxes, and relations. The policy π_θ is trained on spatially grounded VQA samples from STVQA-7K
 427 C using our multi-objective spatial reward R (Section 2.1), which enforces structural validity, count
 428 fidelity, answer accuracy, and precise spatial grounding.

429 C STVQA-7K: Dataset Construction

430 High-quality spatial VQA datasets remain scarce, as most existing benchmarks either lack grounded
 431 scene-graph annotations (i.e., explicit spatial coordinates for objects and relations) or fail to comprehensively
 432 cover both 2D and 3D spatial reasoning categories. Visual Genome [39] provides dense,
 433 human-annotated scene graphs that support strict grounding of both question generation and answer
 434 verification within a unified representational framework. Using Visual Genome, we synthetically
 435 constructed a spatial visual question answering dataset called SPATIALTHINKER Visual Question
 436 Answering dataset i.e., STVQA-7K comprising 7,587 samples, fully grounded in human-annotated
 437 scene graphs [39], which we employed for post-training the SPATIALTHINKER models.

438 The original VG150 predicate set is limited to 50 relations, missing several important categories
 439 such as positional relations (e.g., left, right, beside), distance-based relations (e.g., near, far, next
 440 to), comparative size (e.g., smaller, taller, bigger), orientation (e.g., facing towards/away), and
 441 containment (e.g., inside, beneath). To address this gap, we extended the scene graph relation space
 442 with an additional 34 predicates, ensuring richer spatial coverage in both 2D and 3D reasoning.
 443 Bounding box coordinates are retained in absolute pixel space, rather than normalized values, to
 444 preserve real-world scale and spatial alignment, to enable both improved spatial reasoning and
 445 effective use of CIoU-based supervision during reward optimization. The dataset construction
 446 pipeline proceeds in three stages: (1) synthetic question generation from ground-truth scene graphs,
 447 (2) automated quality filtering with external verification, and (3) scene graph adaptation for regional
 448 alignment with individual questions.

449 **Synthetic Question Generation.** Visual Genome scene graphs serve as our foundational ground
 450 truth, providing object categories, bounding boxes, and relational triplets for over 150,000 images.
 451 We synthetically generate question-answer pairs for a given scene graph data using Claude Sonnet
 452 4 [4], synthesizing multiple-choice questions based on the salient objects and meaningful spatial
 453 relations explicitly present in each graph. Each question-answer pair is accompanied with a rating

454 generated out of 10 and the difficulty level. Our question generation encompasses nine distinct spatial
 455 reasoning categories: spatial relations (above, behind, near, etc.), physical reach and interaction
 456 (holding, touching), comparative size, orientation from specific viewpoints, instance location within
 457 image frames, depth ordering relative to the camera, distance comparisons to reference objects, object
 458 counting, and existence verification. This comprehensive taxonomy spans both 2D and 3D spatial
 459 understanding, providing a broad coverage of visual-spatial reasoning capabilities. To promote robust
 460 perception, we also include questions involving objects that are partially visible or occluded in the
 461 scene, encouraging the model to reason about spatial arrangements and fine-grained details. For each
 462 question, we generate a rating out of 10.

463 **Quality Filtering and Validation.** To en-
 464 sure semantic correctness at scale, we im-
 465 plement a consistency-based verification
 466 procedure using GPT-4o [34] as an exter-
 467 nal validation model. For each generated
 468 question-answer pair, we assess agreement
 469 between the external model and our syn-
 470 thetic ground truth label using a pass@2
 471 criterion. Questions that fail this initial
 472 consistency check undergo additional eval-
 473 uation with two supplementary model re-
 474 sponses. Items for which all four collected
 475 responses disagree with the generated la-
 476 bel are discarded as potentially incorrect
 477 or ambiguous. This filtering process be-
 478 gins with 56,224 initially generated ques-
 479 tions by Claude Sonnet 4 [4]. We select the
 480 10,000 highest-rated samples based on the
 481 questions complexity and rating towards its
 482 contribution to enhance spatial intelligence
 483 as judged by Claude Sonnet 4. Following
 484 consistency filtering, we retain 6,895
 485 training samples and 692 validation sam-
 486 ples (75%), indicating high label reliability.
 487 The final set consists of 50% samples from the relation category, and the remaining 50% distributed
 488 across the eight other categories. To prevent positional bias, answers are uniformly distributed across
 489 options A, B, C, and D. Figure 1 illustrates the distribution of QA types in STVQA-7K, highlighting
 490 the emphasis on spatial relations while maintaining balanced coverage across the remaining reason-
 491 ing categories. Representative examples of generated QA pairs across the nine spatial reasoning
 492 categories are shown in Figure 2, illustrating the diversity of question types in STVQA-7K.

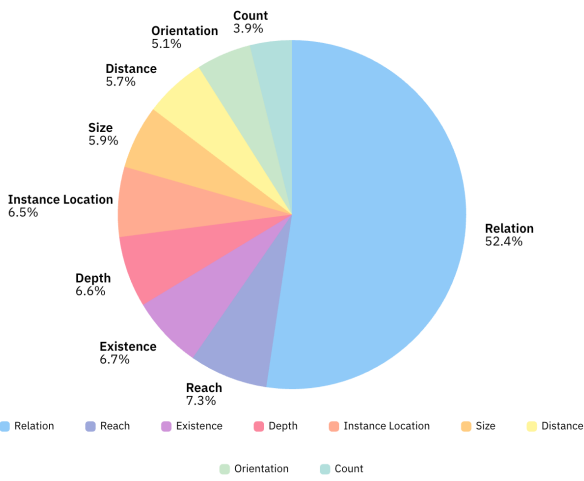


Figure 1: Distribution of QA types in STVQA-7K. The dataset spans a diverse range of spatial reasoning skills, with an emphasis on spatial relations while also balancing other categories such as localization, depth, distance, size, and orientation.

493 **Scene Graph Adaptation.** Since each question focuses on specific objects and relationships within
 494 the broader scene, we derive question-aligned scene subgraphs that capture only the relevant spatial
 495 context. For each question, we extract content words through tokenization and lemmatization to
 496 obtain both singular and plural word forms. We then filter the original scene graph to retain only object
 497 nodes whose labels appear in the extracted question vocabulary. Relational triplets are preserved
 498 when both the subject and object entities are retained and the predicate appears in the question
 499 context. The resulting focused scene graph representations enable training the model to generate
 500 question-aligned region-of-interest subgraphs, encouraging it to localize attention, ground reasoning
 501 in relevant entities and relations, and ultimately learn where to focus within complex visual scenes.

502 D Experimental Setup Details

503 This section presents comprehensive evaluations of SPATIALTHINKER across multiple spatial rea-
 504 soning benchmarks, demonstrating the effectiveness of our multi-objective dense reward design and
 505 data-efficient training approach.

STVQA-7K QA Examples

Spatial Relations



- Q. Where is the cap with respect to the glove?
Options:
(A) above
 (B) below
 (C) beside
 (D) behind

Reach



- Q. What is the woman doing with the surfboard?
Options:
 (A) standing on
 (B) carrying over head
(C) holding
 (D) sitting beside

Existence



- Q. Is there a fork touching the food in the picture?
Options:
 (A) yes
(B) no

Depth



- Q. Which is closer to the camera, the pizza or the bottle?
Options:
 (A) bottle
 (B) they are at the same distance
(C) pizza

Instance Location



- Q. In which part of the image is the fork located?
Options:
 (A) bottom left corner
 (B) center
 (C) top left corner
(D) top right corner

Size



- Q. What is the relationship between the boy and the towel in terms of size?
Options:
(A) boy is larger
 (B) they are the same size
 (C) towel is larger

Distance



- Q. Which object is closer to the chair, the lamp or the boy?
Options:
(A) lamp
 (B) boy
 (C) they are equidistant

Orientation



- Q. From the woman's perspective, which direction is the pole?
Options:
 (A) to the left
(B) in front
 (C) to the right
 (D) behind

Count



- Q. How many skis are there in the image?
Options:
 (A) 3
(B) 4
 (C) 6
 (D) 5

Figure 2: Examples of generated QA pairs across the nine spatial reasoning categories in STVQA-7K. Each category highlights distinct reasoning skills, ranging from relative spatial relations and depth ordering to distance, size, orientation, reach, location, count and existence.

506 **D.1 Implementation Details**

507 We build SPATIALTHINKER upon two strong open-source multimodal base models: Qwen2.5-VL-
508 3B and Qwen2.5-VL-7B [5], using them as backbones for policy optimization with reinforcement
509 learning. No supervised fine-tuning is performed prior to RL training on our STVQA-7K dataset
510 (Section C). We employ GRPO [62] as the advantage estimator as described in Section 2.2, using a
511 rollout size of 8 samples per query and a sampling temperature of 1.0. The models are trained with a
512 maximum context length of 16,384 tokens. The rollout batch size is set to 512, and the global batch
513 size is 128. We train for 75 training steps i.e., 5 training episodes) on $4 \times$ NVIDIA H100 80GB
514 GPUs. Training time totals around 13 hours for the 3B model and 15 hours for the 7B model.

515 The models are trained on high-resolution image inputs ranging from 512×512 to 2048×2048 pixels,
516 to preserve fine-grained spatial information. All model parameters, including the vision encoder,
517 are updated during training. We use the AdamW optimizer with bf16 precision, a learning rate of
518 1×10^{-6} , and a weight decay of 1×10^{-2} . The KL penalty coefficient is set to 10^{-2} . STVQA-7K is
519 partitioned with a 90/10 train-validation split.

520 **D.2 Experimental Setup**

521 We evaluate SPATIALTHINKER across diverse spatial understanding benchmarks, covering both 2D
522 and 3D understanding aspects to assess fine-grained spatial reasoning capabilities and real-world
523 generalization. We compare against both proprietary and open-source baselines, including models
524 specifically trained for spatial reasoning tasks. Our experiments address two key questions: (Q1) Does
525 our spatial VQA data generation pipeline combined with dense reward RL improve MLLMs’ general
526 spatial reasoning capabilities? (Q2) How effectively can MLLMs learn spatial understanding from just
527 7K synthetic training samples, and how does this compare to models trained on orders-of-magnitude
528 larger datasets?

529 **Benchmarks.** We evaluate models across a diverse suite of six spatial reasoning benchmarks that
530 collectively probe both two-dimensional and three-dimensional understanding in MLLMs. CV-Bench
531 [67] measures 2D spatial relations, object counting, depth ordering, and distance reasoning. BLINK’s
532 Spatial Relations and Relative Depth tasks [21] test directional and positional understanding, and
533 fine-grained point-level depth perception—particularly challenging as SPATIALTHINKER receives no
534 explicit point-level supervision during training. 3DSRBench [51] assesses egocentric 3D spatial rea-
535 soning via relational and multi-object comparisons. MMVP [68] examines visual pattern recognition
536 across attributes such as orientation, positional relations, existence, viewpoint, and size. Spatial-
537 Bench [6] assesses general spatial comprehension across counting, existence, positional relationships,
538 physical interactions such as reach, and size comparisons. Finally, RealWorldQA [76] serves as an
539 out-of-distribution evaluation, testing real-world visual reasoning that requires integrating visual
540 information with commonsense knowledge, multi-step reasoning, and practical scene understanding
541 over natural scenes. Together, these benchmarks provide comprehensive, multi-granular evaluation
542 of spatial cognition in multimodal models.

543 **Closed-Source MLLM Baselines.** We compare against widely used closed-source multimodal
544 models including: GPT-4o [34], Claude 3.5 Sonnet [4], and Gemini 2.0 Flash (both standard and
545 “thinking” variants) [25], representing state-of-the-art commercial MLLMs. These models serve as
546 upper reference points for spatial reasoning performance under proprietary settings.

547 **Open-Source MLLM Baselines.** We compare against generalist open-source MLLMs including
548 Qwen2.5-VL 3B and 7B models [5], LLaVA-NeXT [41], Cambrian-1 [67], and VLAA-Thinker [10].
549 These models represent state-of-the-art vision-language architectures, offering strong general visual
550 reasoning but without specific spatial tuning.

551 **Open-Source Spatial MLLM Baselines.** We benchmark against specialized open-source models
552 designed for spatial reasoning: SpaceLLaVA-13B (a public reimplementation of SpatialVLM [8]),
553 SpatialLLM-8B [52] (multi-stage 3D-informed tuning of LLaVA), SpatialRGPT-7B [13] (with depth
554 inputs and region-level spatial enhancements), and RoboPoint-13B [83], which instruction-tunes an
555 MLLM to predict image key-point affordances for robotics and spatial affordance tasks.

556 In addition to the above, we compare against our training variants including supervised fine-tuning
557 (SFT) baselines and vanilla GRPO trained with sparse rewards (accuracy and format only) to isolate
558 the contribution of our dense spatial reward framework.

559 **Evaluation Setting.** We report accuracy as the primary evaluation metric across all tasks. For
560 model outputs, we use greedy decoding (temperature = 0.0, max_new_tokens = 2048) to ensure
561 deterministic generation. Our evaluation infrastructure builds upon OpenVLThinker’s evaluation
562 pipeline [18], adapted to support our new benchmark and dataset formats. For proprietary models,
563 open-source models, and spatial baselines, we conduct zero-shot evaluations on all benchmarks. For
564 SpatialRGPT-7B, we include depth inputs in line with its original training setup. For all other models,
565 only RGB images are used.

566 **D.3 SpatialThinker Prompt Format**

567 We use a structured prompt to guide the model through a four-stage reasoning process, explicitly
568 separated using the tags `<observe>`, `<scene>`, `<think>`, and `<answer>`. This format is enforced
569 during training via a binary format reward $R_f \in \{0, 1\}$, with weight $w_{\text{format}} = 0.1$, which verifies
570 the presence, ordering, and validity of all required tags. The `<scene>` section must contain a JSON-
571 encoded subgraph with object IDs, bounding boxes, and relational triplets, while the final answer
572 must be clearly placed within the `<answer>` tags.

573 Each prompt also includes the input image dimensions in the form `Image size: {Width} × {Height}`,
574 which are dynamically replaced with actual values. Including this information helps the
575 model constrain predicted bounding box coordinates within image bounds, enabling better spatial
576 localization. These coordinates are directly evaluated using IoU-based spatial rewards such as
577 Complete IoU (CIoU), making dimension-aware prediction essential for optimizing structured spatial
578 grounding.

579 **SpatialThinker Prompt**

You FIRST observe the image in `<observe>` `</observe>` tags, then visualise the relevant scene
graph in `<scene>` `</scene>` tags, followed by thinking about the reasoning process as an internal
monologue within `<think>` `</think>` tags and then provide the final answer. The final answer
MUST BE put within `<answer>` `</answer>` tags, and only return the final choice including the
correct option and answer within the answer tags, e.g., `<answer>` (C) The red cube is left of the
green sphere `</answer>`.

Image size: {Width} × {Height}

580 **D.4 Details on SFT Training**

581 To establish a comprehensive baseline for comparison with our reinforcement learning approach, we
582 conduct supervised fine-tuning (SFT) experiments using the same base models (Qwen2.5-VL-3B
583 and Qwen2.5-VL-7B) and training dataset (STVQA-7K). The SFT implementation utilizes LLaMA-
584 Factory framework [85] with Low-Rank Adaptation (LoRA) for parameter-efficient fine-tuning.

585 The training configuration employs LoRA with rank 8 applied to all available modules within the
586 model architecture, enabling comprehensive adaptation while maintaining computational efficiency.
587 Models are trained for 3 epochs totaling 645 training steps, using a context window length of 2048
588 tokens. We adopt BF16 mixed precision training with a learning rate of 1×10^{-4} , following a cosine
589 learning rate schedule with a warmup ratio of 0.1.

590 For the SFT experiments, we train models directly on question-answer pairs without intermediate
591 reasoning traces or chain-of-thought prompting. This design choice reflects the practical constraint
592 that generating ground-truth reasoning traces would require substantial additional dataset processing
593 and annotation. In contrast, reinforcement learning approaches with verifiable rewards (RLVR)
594 naturally enables training with answer supervision alone, as the model learns to generate its own
595 reasoning strategies through environmental feedback rather than imitating pre-specified reasoning
596 patterns.

597 The SFT baseline serves a critical role in our experimental evaluation, providing direct evidence of
598 the generalization advantages offered by reinforcement learning with dense spatial rewards compared
599 to traditional supervised learning on the same dataset.

600 **D.5 Details on RL Training**

601 We implement reinforcement learning training using the EasyR1 framework [84], building upon
602 Qwen2.5-VL-3B and Qwen2.5-VL-7B as base models without any prior supervised fine-tuning. This
603 direct application of RL to the base models enables us to isolate the effects of reward-driven learning
604 from potential confounding factors introduced by intermediate training stages.

605 The training employs Group Relative Policy Optimization (GRPO) [62] as the advantage estimation
606 method, configured with a rollout size of 8 samples per query at a sampling temperature of 1.0. This
607 configuration balances exploration diversity with computational efficiency, allowing the model to
608 discover multiple reasoning strategies while maintaining stable convergence. The training process
609 utilizes a rollout batch size of 512 and a global batch size of 128, processing data through 75 training
610 steps (approximately 5 training episodes) to achieve convergence. The entire training pipeline runs
611 on $4 \times$ NVIDIA H100 80GB GPUs, requiring approximately 13 hours for the 3B model and 15
612 hours for the 7B variant.

613 To preserve fine-grained spatial information critical for accurate object localization and spatial
614 reasoning, models process high-resolution image inputs ranging from 512×512 to 2048×2048
615 pixels. The training configuration updates all model parameters including the vision encoder, enabling
616 comprehensive adaptation to spatial reasoning tasks. Optimization employs AdamW with BF16
617 mixed precision, a conservative learning rate of 1×10^{-6} , and weight decay of 1×10^{-2} . The KL
618 penalty coefficient is set to 10^{-2} to prevent excessive divergence from the base model distribution
619 while allowing sufficient exploration for spatial reasoning strategies. The training utilizes a 90/10
620 train-validation split of the STVQA-7K dataset, with a maximum context length of 16,384 tokens to
621 accommodate detailed scene descriptions and reasoning traces.

622 For baseline comparisons, we train vanilla GRPO models (Qwen2.5-VL-3B + Vanilla GRPO and
623 Qwen2.5-VL-7B) using a simplified reward structure consisting solely of accuracy ($w_{acc} = 0.5$)
624 and format rewards ($w_{format} = 0.5$), without the spatial grounding and count penalty components.
625 This configuration represents standard RLVR approaches that rely on sparse final-answer supervision
626 [16, 64, 10]. The full multi-objective reward design employed for SPATIALTHINKER training,
627 incorporating format, count, accuracy, and spatial rewards with lexicographic gating, is detailed in
628 Section 2.1. The substantial performance improvements of SPATIALTHINKER over vanilla GRPO
629 baselines demonstrate the critical importance of dense spatial supervision in teaching models to
630 perform visually-grounded reasoning.

631 **D.5.1 SpatialThinker RL Training Curves**

632 Throughout reinforcement learning, all four reward components: format, accuracy, count, and
633 spatial; demonstrate consistent and interpretable improvement, reflecting stable learning under our
634 lexicographically gated, multi-objective reward structure. The format reward quickly converges early
635 in training, indicating the model learns to produce structurally valid outputs that adhere to the required
636 scene-grounded reasoning format. Accuracy steadily improves across steps, highlighting the model's
637 increasing ability to provide correct answers. Count reward rises consistently, showing that the model
638 learns to focus on predicting only question-relevant objects and relations, rather than describing the
639 entire scene. The spatial reward also improves gradually, indicating better object localization and
640 grounding, as the model increasingly aligns predicted bounding boxes with ground truth annotations.
641 Together, these trends reflect how each reward component scaffolds a different stage of the reasoning
642 process, enforcing structure, correctness, focus, and grounding in tandem.

643 Response length initially declines, then rises again as it begins producing more deliberate, structured
644 reasoning, signaling an “aha moment” where the model starts to produce more deliberate reasoning
645 traces [16, 87]. This emergent behavior suggests the development of internal problem-solving
646 strategies, as the model learns to spend more “thinking time” before answering, consistent with the
647 emergence of self-reflection and structured planning in its spatial reasoning process.

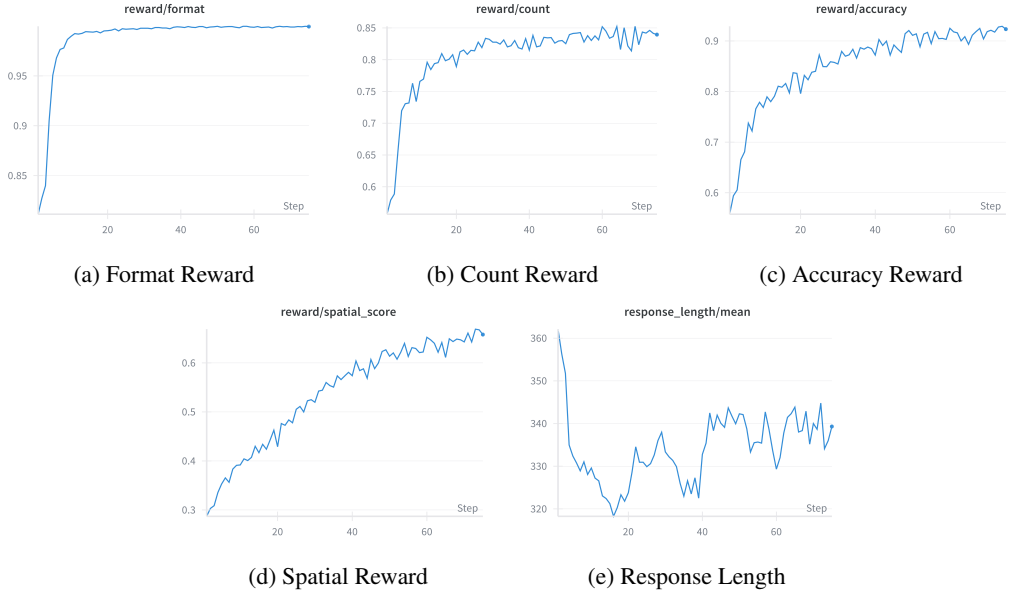


Figure 3: RL training dynamics of SPATIALTHINKER. All reward components (a–d) improve consistently, reflecting stable optimization. Response length (e) shows a non-monotonic trend, indicating emergent reasoning strategies.

648 E Reward Design Rationale

649 Our reward design emerged from iterative refinement to address systematic reward hacking behaviors
 650 observed during training. Early experiments revealed that models readily exploit loopholes in reward
 651 functions—particularly when spatial localization rewards were provided without proper constraints.
 652 This section details our approach to designing a robust reward system that guides models toward
 653 genuine spatial reasoning while preventing degenerate solutions.

654 **Preventing Spatial Reward Hacking.** Our initial reward formulation, which directly rewarded
 655 spatial localization quality, led to unexpected model behavior. Without constraints on generation
 656 quantity, models discovered they could maximize spatial rewards by generating numerous bounding
 657 boxes with varying coordinates. Through Hungarian matching that selects the best-matching boxes,
 658 even random predictions would occasionally yield high Complete IoU (CIoU) scores. This reward
 659 hacking manifested as models producing excessive, hallucinated objects while achieving poor task
 660 accuracy—the spatial reward was inflated despite the clutter of irrelevant predictions degrading actual
 661 performance. To address this exploitation, we introduced the Count Reward that penalizes deviations
 662 from expected object and relation counts. This reward serves dual purposes: (1) preventing reward
 663 hacking by constraining the generation space, and (2) encouraging models to focus on question-
 664 relevant scene elements rather than exhaustively describing the entire image. The count reward
 665 formulation provides a linear penalty proportional to relative deviations from ground truth counts,
 666 normalized to prevent domination by scenes with many objects.

667 **Scene Graph Filtering.** Another form of overfitting emerged when training with complete Visual
 668 Genome scene graphs. Models would memorize exhaustive scene descriptions, including irrelevant
 669 background objects, leading to poor generalization. We addressed this by filtering ground truth scene
 670 graphs to retain only objects and relations relevant to the given question, focusing supervision on
 671 task-critical information.

672 **CIOU over IOU for Spatial Reward.** For spatial localization, we adopt Complete IoU (CIoU)
 673 instead of standard IoU to compute the spatial reward. Unlike IoU, which returns zero when predicted
 674 and ground-truth boxes do not overlap, CIoU provides meaningful gradients by incorporating center
 675 distance, aspect ratio, and overlap [86]. This makes CIoU a denser and more robust supervisory
 676 signal during training.

677 **Balancing Supervision and Exploration.** Our experiments reveal a crucial insight: models learn
 678 simple reward functions significantly faster than complex ones. Tasks with straightforward rewards
 679 (e.g., format compliance) show rapid improvements, while multi-component rewards require careful
 680 balancing. However, counterintuitively, highly detailed reward functions that attempt to supervise
 681 every aspect often degrade performance. Models overfit to maximize minute reward components,
 682 converging to template-style answers that score well on individual metrics while losing flexibility.
 683 We observed accuracy drops mid-training when rewards became too prescriptive, as models focused
 684 on reward optimization rather than genuine task understanding. Effective reinforcement learning
 685 requires providing guidance while preserving exploration space. Our final design addresses this by
 686 providing soft signals through format checks, count constraints, and accuracy rewards, with spatial
 687 localization rewards activated only for correct answers. This maintains the delicate balance between
 688 guidance and exploration necessary for robust learning.

689 **Sequential Optimization via Lexicographic Gating.** To prevent models from gaming individual
 690 reward components at the expense of task accuracy, we implement lexicographic gating [65]. Rewards
 691 are applied in a strict hierarchy: format $\succ \{\text{count}, \text{accuracy}\} \succ \text{spatial}$. This forces models to
 692 first master output formatting, then simultaneously learn to control generation scope and achieve
 693 correctness, before optimizing spatial grounding:

$$R_{\text{total}} = \mathbb{I}[R_{\text{format}} > 0] \cdot (w_f R_f + w_c R_c + w_a R_a + \mathbb{I}[R_{\text{accuracy}} > 0] \cdot w_s R_s) \quad (3)$$

694 where $\mathbb{I}[\cdot]$ is the indicator function, with weights $w_{\text{format}} = 0.1$, $w_{\text{count}} = 0.2$, $w_{\text{accuracy}} = 0.5$,
 695 $w_{\text{spatial}} = 0.2$. This gated design ensures spatial rewards are only applied when the final answer is
 696 correct, aligning grounding quality with task success and preventing scenarios where models achieve
 697 high spatial scores through precise but irrelevant localizations.

698 **F Detailed Results: CV-Bench**

Model	CV-Bench Tasks [67]				CV-Bench		Avg.
	Count	Relation	Depth	Distance	2D	3D	
<i>Proprietary Models</i>							
GPT-4o [34]	65.9	85.7	87.8	78.2	75.8	83.0	79.4
Gemini-1.5-Pro [24]	70.4	85.2	82.4	72.8	77.8	77.6	77.7
Claude 3.7 Sonnet [2]	-	74.2	85.8	84.2	-	85.0	-
<i>Open-Source General MLLMs</i>							
Qwen2-VL-2B [71]	54.7	22.6	16.7	31.7	38.7	24.2	31.5
Qwen2.5-VL-3B [5]	61.5	58.3	67.3	53.0	59.9	60.2	60.1
Qwen2.5-VL-7B [5]	55.9	82.2	70.0	66.0	69.1	68.0	68.6
VLAA-Thinker-3B [10]	61.6	83.5	53.0	46.8	72.6	49.9	61.3
VLAA-Thinker-7B [10]	47.0	74.6	61.3	59.2	60.8	60.3	60.6
LLaVA-NeXT-34B [41]	-	-	-	-	73.0	74.8	73.9
Mini-Gemini-HD-34B [44]	-	-	-	-	71.5	79.2	75.4
Cambrian-1-34B [67]	-	-	-	-	74.0	79.7	76.9
<i>Open-Source Spatial MLLMs</i>							
Spatial-LLaVA-7B [74]	-	-	57.3	52.2	-	54.8	-
VisualThinker-R1-2B [87]	59.6	66.8	54.2	56.7	63.2	55.45	59.3
Spatial-RGPT-7B w/ depth [13]	-	-	62.3	59.0	-	60.7	-
RoboPoint-13B [83]	-	75.6	77.8	44.5	-	61.15	-
SpaceThinker-Qwen2.5-VL-3B [1]	61.0	69.2	70.5	61.3	65.1	65.9	65.5
SpaceLLaVA-13B [8]	-	63.7	66.8	70.2	-	68.5	-
SpatialBot-3B [6]	-	69.4	77.3	60.8	-	69.05	-
<i>Method Comparison (Trained on STVQA-7K)</i>							
Qwen2.5-VL-3B + SFT	30.2	77.5	61.2	75.5	53.9	68.4	61.2
Qwen2.5-VL-3B + Vanilla GRPO	67.5	73.7	64.0	69.2	70.6	66.6	68.6
SpatialThinker-3B	68.5	73.5	79.7	72.8	71.0	76.3	73.7
Qwen2.5-VL-7B + SFT	33.3	78.9	64.8	77.7	56.1	71.3	63.7
Qwen2.5-VL-7B + Vanilla GRPO	58.9	78.8	79.3	73.7	68.9	76.5	72.7
SpatialThinker-7B	68.7	86.7	81.2	76.2	77.7	78.7	78.2

Table 3: Detailed breakdown of CV-Bench [67] results across Count, Relation, Depth, and Distance subtasks.

699 **G Detailed Results: 3DSRBench**

Model	3DSRBench Tasks [51]				Avg.
	Height	Location	Orientation	Multi-Object	
<i>Proprietary Models</i>					
GPT-4o [34]	53.2	59.6	21.6	39.0	44.3
Claude 3.5 Sonnet [3]	53.5	63.1	31.4	41.3	48.2
Gemini 2.0 Flash [25]	49.7	68.9	32.2	41.5	49.9
Gemini 2.0 Flash (thinking) [25]	53.0	67.1	35.8	43.6	51.1
<i>Open-Source MLLMs</i>					
Qwen2.5-VL-3B [5]	45.2	56.8	35.7	35.7	44.0
Qwen2.5-VL-7B [5]	44.1	62.7	40.6	40.5	48.4
Qwen2.5-VL-72B [5]	53.3	71.0	43.1	46.6	54.9
Cambrian-1-8B [67]	23.2	53.9	35.9	41.9	42.2
LLaVA-NeXT-8B [41]	50.6	59.9	36.1	43.4	48.4
VLAA-Thinker-7B [10]	54.0	60.2	42.9	49.1	52.2
<i>Open-Source Spatial MLLMs</i>					
SpatialBot-3B [6]	40.4	54.4	31.9	33.5	41.1
SpaceLLaVA-13B [74]	49.3	54.4	27.6	35.4	42.0
SpatialLLM-8B [52]	45.8	61.6	30.0	36.7	44.9
SpatialRGPT-7B w/ depth [13]	55.9	60.0	34.2	42.3	48.4
SpaceThinker-Qwen2.5-VL-3B [1]	53.1	57.3	41.9	49.6	51.1
<i>Method Comparison (Trained on STVQA-7K)</i>					
Qwen2.5-VL-3B + SFT	51.1	58.3	42.7	48.1	50.8
Qwen2.5-VL-3B + Vanilla GRPO	48.9	57.9	42.5	47.2	50.1
SpatialThinker-3B	52.6	61.8	43.4	49.8	52.9
Qwen2.5-VL-7B + SFT	50.6	66.3	43.8	47.9	53.6
Qwen2.5-VL-7B + Vanilla GRPO	54.3	64.7	45.5	50.4	54.7
SpatialThinker-7B	52.0	70.3	45.5	50.9	56.4

Table 4: Detailed Breakdown of 3DSRBench [51] Height, Location, Orientation, and Multi-Object tasks.